5. R. G. Bergman, P. F. Seidler, T. T. Wenzel, *J. Am. Chem. Soc.* **107**, 4358 (1985).
6. W. A. Kiel, R. G. Ball, W. A. G. Graham, *J. Organomet. Chem.* **383**, 481 (1990); M. Hackett, J. A. Ibers, G. M. Whitesides, *J. Am. Chem. Soc.* **110**, 1436 (1988); T. Gregory, P. Harper, R. S. Shinomoto, M. A. Deming, T. C. Flood, *ibid.*, p. 7915.
7. B. H. Weiller, E. P. Wasserman, R. G. Bergman, C. B. Moore, G. C. Pimentel, *J. Am. Chem. Soc.* **111**, 8288 (1989); E. P. Wasserman, C. B. Moore, R. G. Bergman, *Science* **255**, 315 (1992); R. G. Schultz *et al.*, *J. Am. Chem. Soc.* **116**, 7269 (1994); A. A. Bengali, R. H. Schultz, C. B. Moore, R. G. Bergman, *ibid.*, p. 9585.
8. P. L. Watson, *J. Am. Chem. Soc.* **105**, 6491 (1983); *J. Chem. Soc. Chem. Commun.* **1983**, 276 (1983); P. L. Watson and G. W. Parshall, *Acc. Chem. Res.* **18**, 51 (1985); M. E. Thompson and J. E. Bercaw, *Pure Appl. Chem.* **56**, 1 (1984); M. E. Thompson *et al.*, *J. Am. Chem. Soc.* **109**, 203 (1987); C. M. Fendrick and T. J. Marks, *ibid.* **108**, 425 (1984); J. W. Bruno *et al.*, *ibid.* **110**, 8731 (1986); R. Quignard, C. Lecuyer, A. Choplin, D. Olivier, J. M. Basset, *J. Mol. Catal.* **74**, 353 (1992).
9. P. Burger and R. G. Bergman, *J. Am. Chem. Soc.* **115**, 10462 (1993). Examples of late metal σ-bond metathesis have been observed with arenes and aldehydes; see M. Gomez, D. J. Robinson, P. M. Maitlis, *J. Chem. Soc. Chem. Commun.* **1983**, 825 (1983); M. Gomez, P. I. W. Yarrow, D. J. Robinson, P. M. Maitlis, *J. Organomet. Chem.* **279**, 115 (1985); M. Gomez, J. M. Kisenyi, G. J. Sunley, P. M. Maitlis, *ibid.* **296**, 197 (1985); H. Lemkuhl, M. Bellenbaum, J. Grundke, *ibid.* **330**, C23 (1987); H. Lemkuhl, R. Schwickardi, C. Krueger, G. Rabbe, *Z. Anorg. Allg. Chem.* **581**, 41 (1990); H. Lemkuhl, R. Schwickardi, G. Mehler, C. Krueger, R. Goddard, *ibid.* **606**, 141 (1991). See also R. L. Brainard, W. R. Nutt, R. T. Lee, G. M. Whitesides, *Organometallics* **7**, 2379 (1988); P. Diversi *et al.*, *J. Chem. Soc. Dalton Trans.* **1993**, 351 (1993).
10. M. Brookhart, B. Grant, J. Volpe, *Organometallics* **11**, 3920 (1992).
11. While preparing this report, we were made aware of another recent example of a structurally characterized η^1-CH_2Cl_2 metal complex, $[(P(^iPr)_3)_2Pt(H)(ClCH_2Cl)]$-$BAr_f$, which has CH_2Cl_2 bond distances and angles consistent with those found for **2**: M. D. Butts and G. J. Kubas, personal communication. For other η^1-alkyl halide complexes that have been prepared, see M. J. Burk, B. Segmuller, R. H. Crabtree, *Organometallics* **6**, 2241 (1987); R. M. Conroy-Lewis, A. D. Redhouse, S. J. Simpson, *J. Organomet. Chem.* **366**, 357 (1989); R. J. Kulawiec, J. W. Faller, R. H. Crabtree, *Organometallics* **9**, 745 (1990); D. M. Van Seggen, O. P. Anderson, S. H. Strauss, *Inorg. Chem.* **31**, 3987 (1992); C. H. Winter, W. R. Veal, C. M. Garner, J. A. Gladysz, *J. Am. Chem. Soc.* **111**, 4766 (1989). For reported crystal structures of chelated CH_2Cl_2 adducts, see M. Brown and J. M. Waters, *J. Am. Chem. Soc.* **112**, 2442 (1990); M. R. Colsman, M. D. Noirot, M. M. Miller, D. P. Anderson, S. H. Strauss, *ibid.* **110**, 6886 (1988); M. R. Colsman *et al.*, *ibid.* **112**, 2349 (1990); T. D. Newbound *et al.*, *ibid.* **111**, 3762 (1989); D. M. Van Seggen, P. K. Hurlbart, O. P. Anderson, S. H. Strauss, *ibid.* **114**, 10995 (1992).
12. R. J. Myers and W. D. Gwinn, *J. Chem. Phys.* **20**, 1420 (1952).
13. A 0.010 M solution of **2** in CD_2Cl_2 under 1 atm of $^{13}CH_4$ was monitored by ^{1}H NMR spectrometry at 10°C. Conversion to an equilibrium mixture of **2** and ^{13}C-**2** followed pseudo-first-order kinetics (observed rate constant $k_{obs} = 2.40 \times 10^{-4}$ s^{-1}; half-life = 50.1 min).
14. B. B. Wayland, A. E. Sherry, *J. Am. Chem. Soc.* **113**, 5305 (1991); X. X. Zhang and B. B. Wayland, *ibid.* **116**, 7897 (1994).

15. Supported by the Director, Office of Energy Research, Office of Basic Energy Sciences, Chemical Sciences Division, of the U.S. Department of Energy under contract DE-AC03-7600098. Determination of the solid-state structure of **2** was carried out by F. J. Hollander, director of the U.C. Berkeley x-ray diffraction facility (CHEXRAY). We acknowledge a generous loan of iridium chloride from Johnson Matthey Aesar/Alfa Co.

8 August 1995; accepted 14 November 1995

Direct Perception of Three-Dimensional Motion from Patterns of Visual Motion

Cornelia Fermüller and Yiannis Aloimonos*

Measurements of retinal motion along a set of predetermined orientations on the retina of a moving system give rise to global patterns. Because the form and location of these patterns depend purely on three-dimensional (3D) motion, the effects of 3D motion and scene structure on image motion can be globally separated. The patterns are founded on easily derivable image measurements that depend only on the sign of image motion and do not require information about optical flow. The computational theory presented here explains how the self-motion of a system can be estimated by locating these patterns.

To detect the image of movement is the first task of all systems with vision, and to reach an understanding of movement is a primary goal of all later perceptual analysis (*1*), for animals as well as in robots. Although an organism or a mechanism may move in a nonrigid manner as a whole, with the head, arms, legs, wings, or wheels undergoing different motions, the eyes move rigidly—that is, as a sum of an instantaneous translation and rotation. Thus, the images perceived on the retina of the eye (or on the film in a camera) originate from a rigid motion.

The fundamental, abstract geometric concept used to describe the computational analysis of visual motion is that of the two-dimensional (2D) motion field: As a system moves in its environment, every point of the environment has a velocity vector with respect to the system. The projection of these 3D velocity vectors on the retina of the system's eye constitutes the so-called motion field. This field depends on the 3D motion and the structure of the scene in view. If a spherical eye moves with a translation **t**, the motion field is along the great circles containing the vector **t** (Fig. 1A), pointing away from the focus of expansion (FOE) and toward the focus of contraction (FOC). The points FOE and FOC are the points where **t** cuts the image sphere. If the eye rotates with a velocity **ω** (Fig. 1B), the motion field is along the circles resulting from the intersection of the image sphere with planes perpendicular to the rotation axis; this axis cuts the sphere at points AOR (axis of rotation) and −AOR. For general rigid motion, the motion field on the sphere is the addition of a translational field and a rotational field (Fig. 1C). In this case, the motion field does not have a simple structure, and it becomes difficult to locate the points FOE and AOR, that is, to solve the problem of determining a system's 3D motion (its egomotion) with the 2D motion field as input (*2*).

This difficulty is compounded because the information that can be derived from the sequence of images sensed by the moving retina is not the exact projection of the 3D motion field, but rather only information about the movement of light patterns. The exact movement of every point on the image is termed the optical flow field. In general, accurate values of the optical flow field are not computable; the so-called normal flow, the component perpendicular to the edges, is the only component of the optical flow that is well defined on the basis of local information. This is the well-known aperture prob-

Computer Vision Laboratory, Center for Automation Research, Department of Computer Science and Institute for Advanced Computer Studies, University of Maryland, College Park, MD 20742–3275, USA.

*To whom correspondence should be addressed.

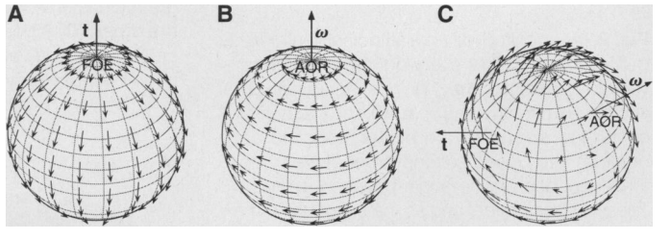

Fig. 1. Motion fields on a spherical retina. The image **r** of a scene point with position vector **R** (with regard to an orthonormal coordinate system fixed to the center *O* of the unit sphere) is formed by perspective projection through *O*. The sphere undergoes a rigid motion with translational velocity **t** and rotational velocity **ω**. (**A**) Translational motion field. At every point **r**, the motion vector is $(1/|\mathbf{R}|)[(\mathbf{t} \cdot \mathbf{r})\mathbf{r} - \mathbf{t}]$, where $|\mathbf{R}|$ is the length of **R** and "·" denotes the inner vector product. Thus, the motion vector is parallel to the great circle passing through points FOE and FOC, and its value is inversely proportional to the distance to the corresponding scene point. (**B**) Rotational motion field. At every point **r**, the motion vector is $-\boldsymbol{\omega} \times \mathbf{r}$, where "×" denotes the outer vector product. Thus, the motion vector is parallel to the circle passing through **r** perpendicular to **ω**, and it does not depend on the scene in view. (**C**) General rigid motion field. At every point **r**, the motion vector is $(1/|\mathbf{R}|)[(\mathbf{t} \cdot \mathbf{r})\mathbf{r} - \mathbf{t}] - \boldsymbol{\omega} \times \mathbf{r}$.

lem. In many cases, it is possible to obtain additional flow information for areas (patches) in the image. Thus, the input that any system can use for further motion processing is some partial optical flow information. Our analysis is based on a minimum amount of knowledge about image motion, namely the sign of the projection of optical flow along directions where it can be robustly computed. These measurements along a set of appropriately chosen orientations possess a rich global structure; they give rise to simple patterns in the image surface, and the location and form of these patterns encode the 3D motion parameters independently of the depth of the scene in view. The selected orientations are defined below.

Two classes of orientations are defined with regard to an axis. Consider an axis **s** passing through the center of a spherical eye and cutting the sphere at points N and S. The unit vectors tangential to the great circles containing **s** define a direction for every point on the retina (Fig. 2A, left). These orientations are called **s**-longitudinal. Similarly, the **s**-latitudinal orientations are defined as the unit vectors tangential to the circles resulting from the intersection of the sphere with planes perpendicular to the axis **s** (Fig. 2A, right).

Some properties of these directions will be of use later. Consider the two axes $\mathbf{s}_1$ (N_1S_1) and $\mathbf{s}_2$ (N_2S_2). Each axis defines at every point a longitudinal and a latitudinal direction. The locus of points on the sphere where the $\mathbf{s}_1$-longitudinal directions are perpendicular to the $\mathbf{s}_2$-longitudinal directions (or where the $\mathbf{s}_1$-latitudinal directions are perpendicular to the $\mathbf{s}_2$-latitudinal directions) constitutes two quadratic curves whose geometry is explained in Fig. 2B (left). Similarly, the longitudinal directions of one axis and the latitudinal directions of the other axis are perpendicular to each other along the great circle defined by $\mathbf{s}_1$ and $\mathbf{s}_2$ (Fig. 2B, right).

The structure of the projections of a rigid motion field on the **s**-longitudinal and **s**-latitudinal vectors is examined by studying how the sign of these projections is related to the 3D motion, because the sign of flow is the information used as input to the motion interpretation process. For this purpose, we adopt the following definitions of the directions: **s** (NS)–longitudinal vectors are called positive if they point away from N, negative if they point away from S, and zero otherwise. Similarly, **s**-latitudinal vectors are called positive if their direction is counterclockwise with respect to **s**, negative if their direction is clockwise, and zero otherwise (Fig. 2C). Because a rigid motion field is the addition of a translational and a rotational field, the cases of pure translation and pure rotation are first considered separately.

If the observer moves with a pure translation of velocity **t**, the motion field on the sphere is along the direction of the **t**-longitudinal vectors (Fig. 1A). If the translational motion field of Fig. 1A is projected on the **s**-longitudinal vectors of Fig. 2A, the resulting vectors will be zero, positive, or negative. The vectors will be zero on two second-order curves (symmetric around the center of the sphere) whose shape depends on the angle between the vectors **t** and **s** (Fig. 2B, left). The area inside the curves will contain negative vectors, and the area outside the curves will contain positive vectors (Fig. 3A).

If the observer moves purely rotationally with velocity **ω**, the motion field on the sphere is along the direction of the **ω**-latitudinal vectors (Fig. 1B). If the rotational motion field of Fig. 1B is projected on the **s**-longitudinal vectors of Fig. 2A, the resulting vectors will be zero, positive, or negative. The vectors will be zero on the great circle defined by **s** and **ω**, positive in one hemisphere, and negative in the other (Fig. 3B).

If the observer translates with velocity **t** and rotates with velocity **ω**, the projection of the general motion field on any set of **s**-longitudinal vectors can be classified for parts of the image. If at a longitudinal vector the projection of both the translational

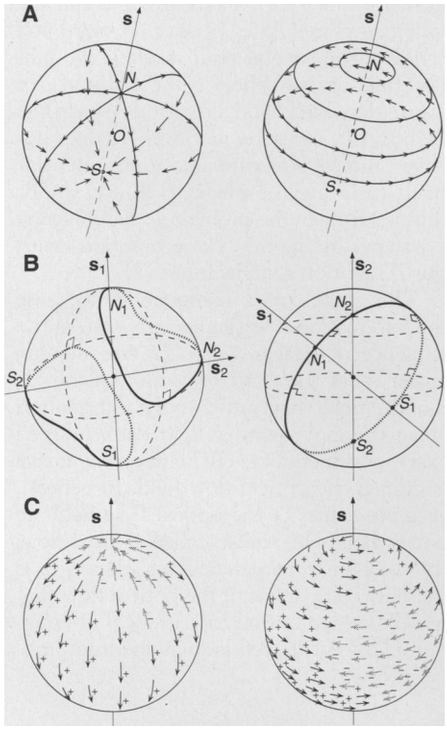

Fig. 2. (**A**) Longitudinal and latitudinal vector fields defined by axis **s**. At every point **r**, a longitudinal vector has direction $(\mathbf{s} \cdot \mathbf{r})\mathbf{r} - \mathbf{s}$, and a latitudinal vector has direction $-\mathbf{s} \times \mathbf{r}$. (**B**) The great circles containing $\mathbf{s}_1$ and $\mathbf{s}_2$ are perpendicular to each other on two closed second-order curves whose form depends on the angle between $\mathbf{s}_1$ and $\mathbf{s}_2$. These curves are defined as the set of points **r** for which $(\mathbf{s}_1 \times \mathbf{r}) \cdot (\mathbf{s}_2 \times \mathbf{r}) = 0$ or $(\mathbf{s}_1 \cdot \mathbf{r})(\mathbf{s}_2 \cdot \mathbf{r}) = \mathbf{s}_1 \cdot \mathbf{s}_2$. The $\mathbf{s}_1$-longitudinal vectors are perpendicular to the $\mathbf{s}_2$-latitudinal vectors along the great circle through $\mathbf{s}_1$ and $\mathbf{s}_2$, defined as $(\mathbf{s}_1 \times \mathbf{s}_2) \cdot \mathbf{r} = 0$. (**C**) Positive and negative longitudinal and latitudinal image motion measurements. The input used in the motion interpretation process is the sign of the image motion's value in longitudinal and latitudinal directions.

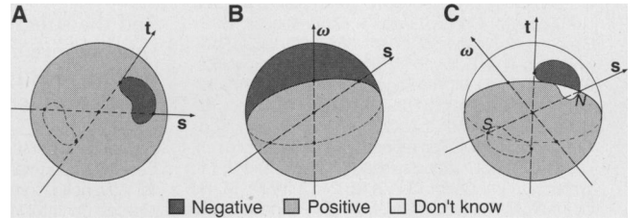

Fig. 3. **s**-Longitudinal pattern. (**A**) At every point **r**, the projection of the translational motion vector on the **s**-longitudinal vector is $(1/|\mathbf{R}|)$ $[(\mathbf{t} \cdot \mathbf{r})\mathbf{r} - \mathbf{t}] \cdot [(\mathbf{s} \cdot \mathbf{r})\mathbf{r} - \mathbf{s}] = (1/|\mathbf{R}|)[\mathbf{s} \cdot \mathbf{t} - (\mathbf{s} \cdot \mathbf{r})(\mathbf{t} \cdot \mathbf{r})]$. It is zero on the curves $\mathbf{s} \cdot \mathbf{t} = (\mathbf{s} \cdot \mathbf{r})(\mathbf{t} \cdot \mathbf{r})$ (as shown in Fig. 2A), negative inside the curves, and positive outside the curves. (**B**) At every point **r**, the projection of the rotational motion vector on the **s**-longitudinal vector is $-(\boldsymbol{\omega} \times \mathbf{r}) \cdot [(\mathbf{s} \cdot \mathbf{r})\mathbf{r} - \mathbf{s}] = (\mathbf{s} \times \boldsymbol{\omega}) \cdot \mathbf{r}$. It is zero on the great circle $(\mathbf{s} \times \boldsymbol{\omega}) \cdot \mathbf{r} = 0$ passing through **s** and **ω**, positive in one hemisphere, and negative in the other. (**C**) A general rigid image motion defines a pattern along every **s**-longitudinal vector field: an area of negative values, an area of positive values, and an area of values whose signs are unknown a priori because they depend on the scene.

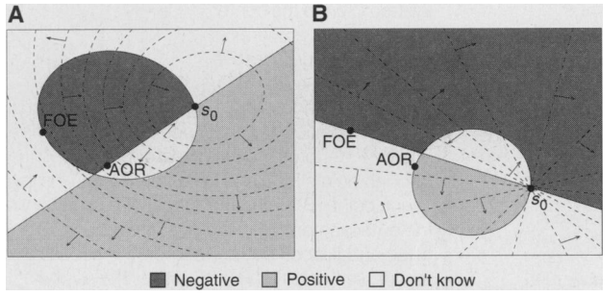

Fig. 4. (**A**) **s**-Longitudinal vectors and (**B**) **s**-latitudinal vectors in a plane, with the patterns superimposed. Note that the "don't know" area contains both positive and negative vectors.

and rotational vectors is positive, then the projection of the image motion (the sum of the translational and rotational vectors) will also be positive. Similarly, if the projections of both the translational and rotational vectors on a longitudinal vector at a point are negative, the projection of the motion vector at this point will also be negative. In other words, if the values along an **s**-longitudinal field (Fig. 3, A and B) are added, whenever positive and positive come together, the result will be positive, and whenever negative and negative come together, the result will be negative. However, whenever positive and negative come together, the result can be either positive or negative. In such a case, the sign of the projection of the rigid motion vector depends on the value of the translational and rotational vector components, and thus on the length of the vectors **t** and ω and the depth of the scene. [Actually, this "don't know" area also contains information regarding 3D motion and structure (*3*).]

The distribution of the sign of image motion along the **s**-longitudinal set of directions thus defines a pattern on the sphere. A pattern like that shown in Fig. 3C is obtained for a general rigid motion field that arises from a translation **t** and a rotation ω on an **s**-longitudinal set of directions. This pattern consists of an area of strictly positive values, an area of strictly negative values, and an area (covering half of the sphere) in which the values are either positive or negative depending on the vectors **t** and **ω** and the depth of the scene. The pattern is characterized by one great circle containing ω and **s** and by two quadratic curves containing the points FOE, FOC, *N*, and *S*. For every pattern, half of the sphere carries valuable information (positive or negative) and the other half does not; however, the locations of these areas are different for different patterns. Consequently, every image point has distinctive information in some pattern.

The pattern of Fig. 3C is independent of the depth of the scene in view and depends only on a subset of the 3D motion parameters. In particular, the great circle is defined by one rotational parameter and the quadratic curve is defined by two translational parameters; thus, the pattern is of dimension three. In summary, for a rigid motion (**t**,ω) for any axis **s** defining a set of directions on the retina, we can identify an area of the imaging surface where the sign of the motion vector along these directions does not depend on the depth of the scene in view. If a rigid motion field is projected on the **s**-latitudinal directions [defined by the vector **s** (*NS*)], another pattern is obtained, which is analogous to the one of Fig. 3C. In this case, the translational latitudi-

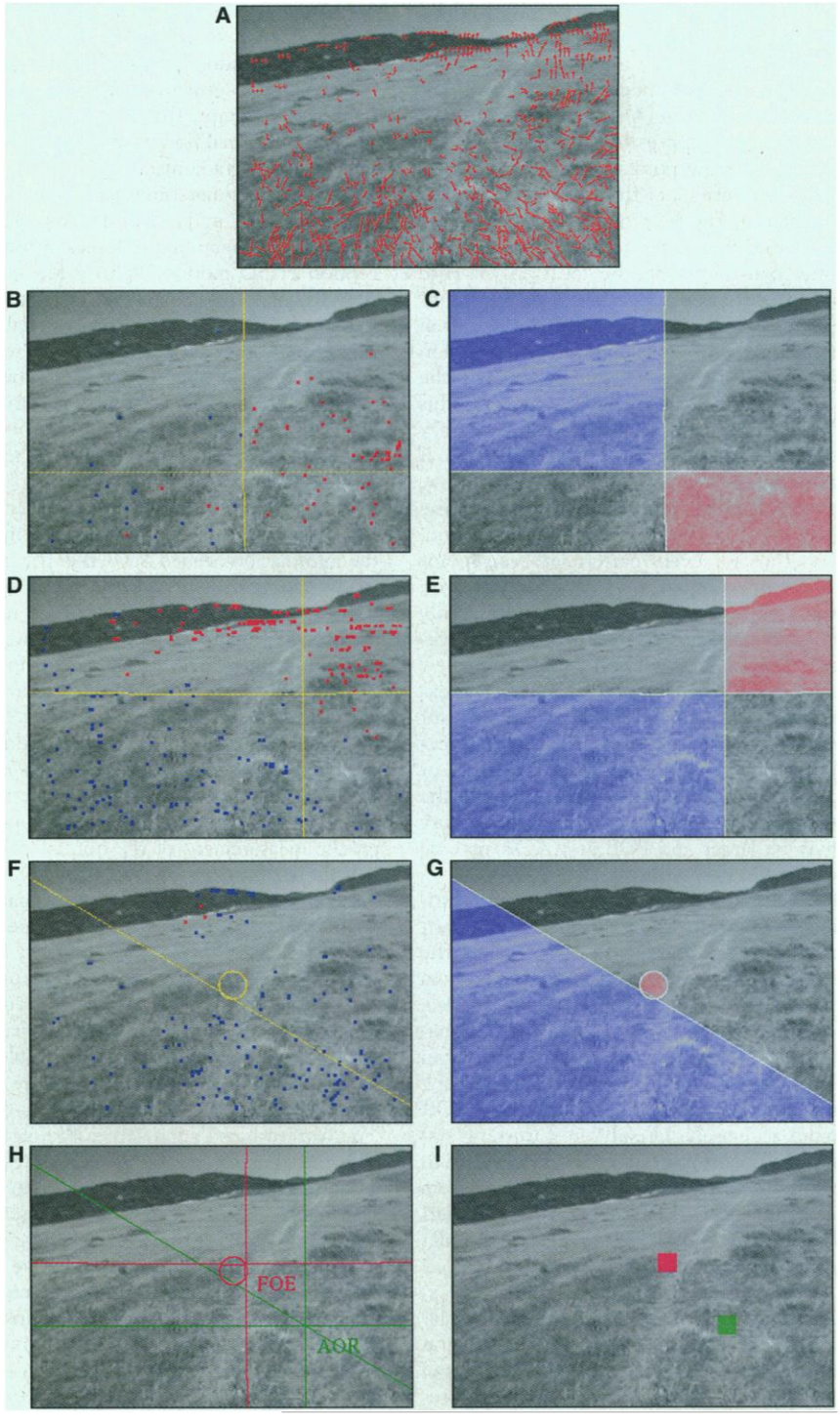

Fig. 5. A camera mounted on an unmanned ground vehicle captured a sequence of images as the vehicle moved along rough terrain, thus undergoing continuously changing rigid motion. (**A**) One frame of the sequence, with the normal flow field overlaid in red. (**B**, **D**, and **F**) Positive (blue) and negative (red) longitudinal vectors corresponding to the *x*, *y*, and *z* axes, respectively. (**C**, **E**, and **G**) Patterns fitted in the final stage after all the patterns have been computed for FOE and AOR at the center of the solution areas shown in (**I**). In (**H**), the boundaries of the patterns whose intersections are FOE and AOR are superimposed on the image. Because measurements are not everywhere available (strong spatial gradients appear sparse), a set of patterns can possibly be fitted with accuracy above the threshold of 97% (where accuracy is defined as the ratio of the number of successfully fitted pixels to the total number of pixels in the pattern). In (I), this fitting results in solutions for FOE and AOR within two bounded areas (red, FOE; green, AOR). The ground truth falls within the estimated areas (*7*).

nal flow is separated into positive and negative by a great circle, and the rotational flow is separated into positive and negative by two closed quadratic curves (as in Fig. 2B) passing from the points AOR, −AOR, N, and S.

The geometric analysis described above allows us to formulate the problem of egomotion estimation as a pattern recognition problem. Assume that the system has the capability of estimating the sign of the retinal motion along a set of directions defined by various **s**-longitudinal or **s**-latitudinal fields. If the system can locate the patterns in each longitudinal and latitudinal vector field, then it has effectively recognized the directions **t** and **ω** (*4*). The intersections of the quadratic curves of the patterns in Fig. 3C provide the points FOE and FOC, and the intersections of the great circles of the patterns in Fig. 3C provide the points AOR and −AOR. Each single pattern provides only constraints on the locations of FOE and AOR, but a collection of patterns constrains these locations to small areas or even to single points. The amount of information available for pattern fitting depends on the computational power of the system, and this information in turn influences the accuracy of the localization of FOE and AOR (*5*). If the system is able to derive optical flow, then it is able to estimate the sign of the projection of the flow along any direction, and thus for every pattern at every point where information is available. If, however, the system is less powerful and can only compute the motion in one direction (normal flow) or the sign of the motion in a few directions, then the solution proceeds exactly as before. The difference is that for each longitudinal or latitudinal set of directions, information (positive, negative, or zero) is not available at every point of the sphere, and consequently the uncertainty may be larger and FOE and AOR may be obtained only within bounds.

After the directions of **t** and **ω** are estimated from the sign of the flow along various directions, the length of **ω** (that is, the exact rotation) can easily be estimated from the values of flow measurements (*6*). Also, after deriving 3D motion from the information supplied by the patterns, the system can estimate optical flow to derive the 3D scene structure and to estimate FOE and AOR more accurately. Usually, in a working system, information from other senses is used in addition. This information may come from inertial sensors, such as gyros and accelerometers in robotic systems or vestibular mechanisms in biological systems.

For the case of a planar retina, the **s**-longitudinal vectors become perpendicular to conic sections defined by the intersection of the image plane with a family of cones of axis **s** (Fig. 4A). Analogously, the **s**-latitudinal vectors become perpendicular to straight lines passing through the intersection s_0 of axis **s** with the image plane (Fig. 4B). The great circle and the second-order curve that characterize the patterns of positive and negative vectors become a straight line and a conic section, respectively.

A part of the theory described here has been implemented and tested on a number of calibrated indoor image sequences, with excellent results (*6*). The solutions for FOE and AOR were always bounded areas that contained the ground truth (*7*) and were not larger than 2° of the visual field. Figure 5 shows an outdoor image sequence experiment with an unmanned ground vehicle. In this experiment, the only input was the sign of the normal flow at image points with strong spatial gradients.

The pattern-matching approach to egomotion estimation does not directly relate to traditional computational studies of the perception of 3D motion. With a few exceptions (*8*), such studies addressed the problem in two steps. In the first step, the optical flow was estimated as an approximation to the motion field; in the second step, the 3D motion was estimated through a local decomposition of the optical flow field (*9–12*). In the scheme described here, the retinal motion information used is equivalent to the sign of the optical flow along some direction. In other words, for a vector **v** on the image, the information needed is whether the image motion along the line defined by the vector **v** has the sign of **v** or −**v**. This is a robust qualitative property of the optical flow, and, as demonstrated here, it is sufficient for the task of egomotion perception when used with the introduced global constraints. It has been argued (*13*) that qualitative estimates of optical flow are often sufficient for many tasks; for instance, the task of detecting a potential crash (*14*) may not even require a precise measurement of the normal component of the flow. As suggested in (*15*), "it is sufficient that the image motion estimate be qualitatively consistent with the perspective 2D projection of the 'true' 3D velocity field. Even estimates that don't correspond to image velocity, like the ones derived by Reichardt's correlation model or equivalent energy models (*16*), may be acceptable for several visual tasks if the estimates are consistent over the visual field" (pp. 131–132). The pattern-based approach to the problem of egomotion estimation demonstrates the feasibility of such ideas about qualitative visual motion analysis. The ideas described here may relate to neuroscience experiments in which primates were found to have cells that respond to patterns of visual motion (*17*), and psychologists may find a link between the patterns described here and the transformational invariants in Gibson's theory (*18*) of direct perception.

REFERENCES AND NOTES

1. Y. Aloimonos and A. Rosenfeld, *Science* **253**, 1181 (1991); Y. Aloimonos and D. Shulman, *Integration of Visual Modules: An Extension of the Marr Paradigm* (Academic Press, Boston, 1993).
2. Computer vision researchers usually refer to egomotion estimation as the problem of recovering FOE and the exact rotation. However, the sign of the flow fields used here allows for the computation of the rotation only up to a constant multiplication factor; that is, only AOR can be derived.
3. C. Fermüller and Y. Aloimonos, *Tech. Rep. CAR-TR-732* (Center for Automation Research, University of Maryland, College Park, 1994).
4. The particular structure of the positive and negative vectors in the "don't know" area (*19*) makes it possible to localize the patterns very efficiently by searching only a small part of the image and using standard computational techniques.
5. The accuracy of the localization of FOE and AOR also depends on the structure of the scene in view. In an analysis of the relation between 3D rigid motion and complete directional motion fields (*20*), it was found that theoretically there is almost always enough information in the direction of motion fields to recover 3D motion uniquely. Ambiguity can occur only for surfaces in view that lie in a particular area bounded by surfaces of a second and third order.
6. C. Fermüller and Y. Aloimonos, *Int. J. Comput. Vision* **15**, 7 (1995); *ibid.* **11**, 165 (1993); C. Fermüller, in Special Issue on Qualitative Vision, Y. Aloimonos, Ed., *ibid.* **14**, 147 (1995).
7. The ground truth was derived from inertial sensor data and from a photogrammetric numerical solution (*9, 11*) that used manual correspondences of image features.
8. J. Aloimonos and C. M. Brown, in *Proc. Workshop on Computer Vision: Representation and Control* (IEEE Computer Society, Annapolis, MD, 1984), pp. 72–77; B. K. P. Horn and E. J. Weldon, in *Proc. International Conference on Computer Vision* (IEEE Computer Society, London, 1987), pp. 2–11.
9. H. C. Longuet-Higgins, *Nature* **293**, 133 (1981).
10. _____ and K. Prazdny, *Proc. R. Soc. London Ser. B* **208**, 385 (1984); J. J. Koenderink, *Vision Res.* **26**, 161 (1986).
11. R. Y. Tsai and T. S. Huang, *IEEE Trans. Pattern Anal. Machine Intell.* **6**, 13 (1984); O. Faugeras and S. Maybank, *Int. J. Comput. Vision* **4**, 225 (1990).
12. S. Ullman, *The Interpretation of Visual Motion* (MIT Press, Cambridge, MA, 1979).
13. A. Verri and T. Poggio, *IEEE Trans. Pattern Anal. Machine Intell.* **11**, 490 (1989).
14. R. C. Nelson and J. Y. Aloimonos, *ibid.* **11**, 1102 (1989).
15. N. Ancona and T. Poggio, in Special Issue on Qualitative Vision, Y. Aloimonos, Ed., *Int. J. Comput. Vision* **14**, 131 (1995).
16. W. Reichardt, in *Principles of Sensory Communication*, W. A. Rosenblith, Ed. (Wiley, New York, 1961), pp. 303–317; *J. Comp. Physiol.* **161**, 533 (1987); T. Poggio and W. Reichardt, *Kybernetik* **13**, 223 (1973); J. P. H. van Santen and G. Sperling, *J. Opt. Soc. Am. A* **1**, 451 (1984).
17. C. J. Duffy and R. H. Wurtz, *J. Neurophysiol.* **65**, 1329 (1991); K. Tanaka and H. A. Saito, *ibid.* **62**, 626 (1989).
18. J. Gibson, *The Ecological Approach to Visual Perception* (Houghton Mifflin, Boston, 1979).
19. C. Fermüller, in *Active Perception*, Y. Aloimonos, Ed. (Erlbaum, Hillsdale, NJ, 1993), pp. 103–150; _____ and Y. Aloimonos, in *Visual Navigation: From Biological Systems to Unmanned Ground Vehicles*, Y. Aloimonos, Ed. (Erlbaum, Hillsdale, NJ, in press).
20. T. Brodsky, C. Fermüller, Y. Aloimonos, *Tech. Rep. CAR-TR-780* (Center for Automation Research, University of Maryland, 1995).

21. Supported by Advanced Research Projects Agency grant DAA H04-93-G-0419, Office of Naval Research grant N00014-93-1-0257, and NSF grant IRI-9057934 (under a Presidential Young Investigator Award).

24 May 1995; accepted 26 October 1995